JOURNAL OF SPACECRAFT AND ROCKETS
Vol. 57, No. 3, May–June 2020

Prospects of a Hybrid Magnetic/Electrostatic Sample Container Retriever

Takuma Shibata*
Graduate University for Advanced Studies, SOKENDAI, Sagamihara 252-5210, Japan
and
Trevor Bennett† and Hanspeter Schaub‡
University of Colorado Boulder, Boulder, Colorado 80309

https://doi.org/10.2514/1.A34509

Martian sample return missions continue to be investigated to improve the understanding of planets. However, rendezvous and docking in deep space requires autonomous navigation and control capabilities. A deep-space satellite cannot be controlled by an Earth-based ground station in real time. As a solution of this deep-space docking challenge, the prospects of a sample container retriever using an electrostatic force and a flux pinning force are discussed in this paper. The proposed method uses the electrostatic interaction to retrieve an orbit sample (OS) container launched from a planet by a small rocket. The cylindrical OS studied in this research has three permanent magnets. To perform rendezvous and docking with the OS safely, a Martian sample return orbiter controls the angular velocity and attitude of the OS using electrostatic control when the sample is multiple meters away. When it is less than 1 m away, it is tugged to the orbiter and docked safely using the flux pinning effect. The feasibility of the proposed retrieval system is discussed from the aspects of the required electrical energy and the local space weather Debye length. To detumble the motion of the OS, a nonlinear controller is designed using a Lyapunov function as well as the Mukherjee and Chen theorem. The numerical performance simulations illustrate the feasibility and prospects of this method.

Nomenclature

$\boldsymbol{B}_m$	=	magnetic flux density of permanent magnets on an orbit sample container, $\mathrm{Wb/m^2}$
E	=	electric field, V/m
E_{ex}	=	energy for external emission, eV
E_{tr}	=	energy for transfer operation, eV
$\boldsymbol{F}_{f,m}$	=	magnetic force working on a permanent magnet due to mirror images, N
$\boldsymbol{F}_{L,s}$	=	Lorentz force on an orbit sample container, N
$\boldsymbol{F}_p$	=	pinning force, N
$\boldsymbol{H}_{f,m}$	=	magnetic field of mirror images, which are frozen and mobile images, A/m
I	=	current, $\mathrm{A/m^2}$
I_{SEE}	=	secondary effect current, $\mathrm{A/m^2}$
I_{tr2}	=	transfer current, $\mathrm{A/m^2}$
J	=	inertia, $\mathrm{kg \cdot m^2}$
k_c	=	Coulomb's constant, $(\mathrm{N \cdot m^2})/\mathrm{C^2}$
$\boldsymbol{L}$	=	torque, $\mathrm{N \cdot m}$
$\boldsymbol{M}_{f,m}$	=	magnetic moment of mirror images, which are frozen and mobile images, $\mathrm{A \cdot m^2}$
$\boldsymbol{M}_p$	=	magnetic moment of a permanent magnet, $\mathrm{A \cdot m^2}$
n	=	density, $1/\mathrm{cm^3}$
P_{ex}	=	power for external emission, W
P_{tr}	=	power for transfer operation, W
q	=	charge, C
$\boldsymbol{R}_A$	=	radius of body A, m
$\boldsymbol{r}_{\mathrm{FC}}$	=	field cooling position vector from surface of a type-II superconductor to a permanent magnet, m
$\boldsymbol{r}_{f,m}$	=	position vector from mirror images to a permanent magnet, m
$\boldsymbol{r}_{i,j}$	=	position vector from sphere i to sphere j, m
T	=	temperature, eV
$\boldsymbol{v}$	=	relative velocity between an orbit sample container and an orbiter, m/s
ϵ_0	=	permittivity of vacuum, $(\mathrm{N \cdot m^2})/\mathrm{C^2}$
θ	=	Euler angle, deg
λ_D	=	Debye length, m
μ_0	=	permeability of vacuum, $\mathrm{N/A^2}$
ϕ	=	potential, V
ω	=	thermal velocity, m/s

Subscripts

e	=	electron
i	=	ion
o	=	orbiter
ph	=	photoelectron
s	=	orbital sample container

Received 26 March 2019; revision received 19 November 2019; accepted for publication 24 December 2019; published online 27 February 2020.

*Ph.D. Candidate, Department of Space and Astronautical Science, Kanagawa; ts761943is_as@ac.jaxa.jp. Student Member AIAA.

†Ph.D. Candidate, Aerospace Engineering Sciences, 431 UCB, ECNT 320; trevor.bennett@colorado.edu. Student Member AIAA.

‡Associate Professor, Aerospace Engineering Sciences, 431 UCB, ECNT 320; hanspeter.schaub@colorado.edu. Senior Member AIAA.

I. Introduction

RETURNING samples from a planet provide an opportunity for new insights related to the formation and configuration of the planet. HAYABUSA succeeded in bringing particles from the asteroid Itokawa. In recent years, space agencies and companies are looking at Martian sample return missions [1–5]. Unlike the HAYABUSA mission, an explorer cannot get samples by landing the large return vehicle because of the large fuel requirement to escape the planet's gravity. In the Martian sample return missions, it has been proposed that an orbit sample (OS) container is launched using a Mars ascent vehicle (MAV) after samples are collected by the Mars 2020 rover [6–8]. After launching the OS to orbit, a Martian sample return (MSR) orbiter takes it back to the Earth and jettisons the OS protected by an Earth reentry capsule [9–11]. However, the rendezvous and docking of an orbiter to catch the OS are challenging and unsolved aspects of the current mission architecture. An automatic system is desired for the rendezvous docking with the OS because the time lag inhibits real-time communications between an Earth-based ground station and the Mars orbiter [6]. Several docking ideas have been considered to date. In the Mars 2020 mission, the MSR orbiter has a camera to detect

the OS at a distance of 10,000 km. Moreover, the OS has an uhf beacon to help to inform the MSR with an alternate relative range measurement [3,6].

A method using a mechanical structure has been considered to catch the OS on Martian orbits [12,13]. This system mainly consists of a capture cone and lid. The lid starts to close when the OS enters into the capture cone. In addition to using a mechanical structure, an automated rendezvous docking method using the flux pinning force has also been researched [14]. This rendezvous docking method is considered as one of the solutions to capture the OS on orbit in the Mars 2020 mission. The OS that might be used in the Mars 2020 mission is designed to be a spherical shape. Multiple permanent magnets are put on the surface of the OS, and an orbiter has a type-II superconductor. The rendezvous docking method can be conducted safely by controlling the relative distance and velocity between the OS and the orbiter due to the flux pinning effect [3,5,14].

However, a cylindrical OS has more advantages than the spherical shape because it provides better packing for cylindrical sample return cases. In addition, the shape provides a benefit to a Mars ascent vehicle. The cylindrical shape can be designed to optimally fit the fairing of the MAV rather than spherical shape. In the future, it will be required to get more samples at one time. If multiple samples are returned simultaneously using a spherical OS concept, the MAV radius will get bigger. Here, a cylindrical shape has an advantage by making the return packing easier to implement on a MAV. If a cylindrical OS is used for sample return missions, however, the attitude and angular velocity of the OS must be controlled to dock with the MSR orbiter safely. To solve this problem, this paper focuses on both electromagnetic and electrostatic forces.

Electromagnetics have been considered as a method to control uncooperative objects without mechanical touching. A magnetic capture device has been researched in Ref. [15] for sample return missions from a planet. The magnetic capture device consists of a magnetorquer and a permanent magnet mounted on a spacecraft, and an OS has a permanent magnet on the capture axis. This device enables the control of the attitude and angular velocity of the OS. Eddy current brakes have also been researched for space debris removal and detumbling uncooperative objects. This method is effective to detumble space objects consisting of conducting materials such as aluminum or copper. The angular velocity of space debris is suppressed by controlling magnetic coils mounting on the spacecraft [16,17].

The coulomb force has been also considered to suppress the spin rate of space debris [18–20]. Generally, satellites on orbit are charged up by electrons and protons in the local space plasma environment. The potential of satellites can be controlled using electron and/or ion emission devices. Moreover, satellites can control potential of uncooperative objects such as space debris by shooting ions and electrons onto these objects. Thus, an electrostatic potential difference between an uncooperative object and a satellite can be generated. Uncooperative objects on orbit can be controlled using the coulomb force between satellites without directly touching each other. Even if a space debris object is very large as compared with a satellite operating the detumbling system, the angular momentum can be suppressed [19,20]. An experiment was performed to validate using a coulomb force to suppress the spin rate of space debris [21–23].

To get samples off the surface of another planet, the coulomb detumbling method is used for automated rendezvous docking with the cylindrical OS in this paper. As a new approach for future sample return missions, a rendezvous docking system using the flux pinning force and coulomb force is proposed, as shown in Fig. 1. The purpose of this research is to explore the feasibility of the new automated rendezvous docking system. To perform rendezvous docking safely with a cylindrical sample container on orbit, the coulomb detumbling method is important. As an advantage to using coulomb force for the detumbling method, it is not required that actuators are mounted on a cylindrical OS to stabilize the attitude for rendezvous docking with an orbiter. After detumbling, the flux pinning effect [24] is used for docking in this proposed system. For the docking, type-II superconductors are mounted on the orbiter, and the cylindrical OS has permanent magnets.

The goal of this paper is to explore the feasibility and benefits of the proposed system numerically in terms of the required power to operate the proposed system, the Debye length, and the control system. This paper consists of six sections. The second section discusses the required electrical power to operate the proposed system and the Debye length, which are fundamental parameters for operating the electrostatic force in the plasma environment. Required power levels determine the maximum potential that the orbiter can use to control states of the cylindrical OS. The proposed system must operate within the range of the Debye length because the electrostatic field (E-field) is screened beyond the range. The third section explores the force distribution between the cylindrical OS and the orbiter. This proposed system uses two electromagnetic forces, which are the coulomb force to control the attitude and angular velocity and the flux pinning force, which is used to catch the cylindrical OS automatically in a close distance. The relationship of those forces depending on the relative distance is shown in this section. Nonlinear controller design is discussed in the fourth section, whereas the numerical simulation results are presented in the fifth section.

II. Hybrid Magnetic/Electrostatic Sample Container Retriever

The cylindrical orbital sample container provides an opportunity to effectively capture samples launching from the planets as compared

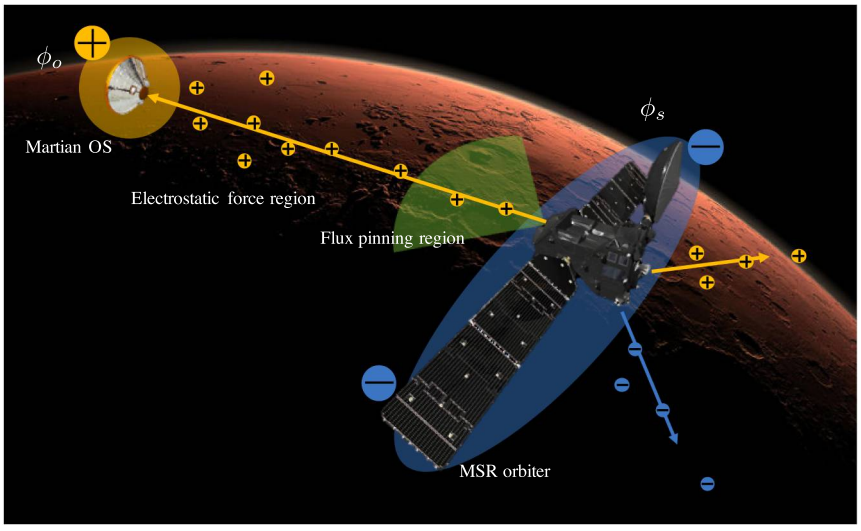

Fig. 1 Hybrid magnetic/electrostatic sample container retriever (orbiter and sample container photograph is courtesy of ESA, and background photograph is courtesy of NASA).

with a conventional spherical sample container. However, the spin rate of the OS should be suppressed for a safe rendezvous docking maneuver because, now, the OS orientation is critical as compared to the spherical container concept. To solve this problem, a hybrid magnetic/electrostatic sample container retriever is proposed. Mainly, this proposed system is operated for two phases, namely, the detumbling phase and the rendezvous docking phase. In the detumbling phase, the spin rate of the OS is suppressed using electrostatic interaction. A Martian sample return orbiter has two electron guns and an ion gun to control the potential of itself, and it has a cylindrical orbital sample container to operate the proposed automated rendezvous docking system on orbit. The potential of the OS is controlled to be constant by getting ions from the ion gun on the orbiter. Another ion gun and electron gun on the orbiter operate to change the potential of the orbiter. These ion and electron guns are controlled to suppress the rotation motion of the OS. For the rendezvous docking phase, the orbiter has type-II superconductors and electromagnetic coils to use flux pinning interface (FPI) [24]. A challenge of the proposed system is that the orbit of the cylindrical OS is limited by the performance of the MAV. On a lower-altitude orbit, the Debye length is small and results in strong Debye shielding of the electrostatic force. Moreover, the shorter Debye length results in a higher power requirement to control the surface potentials. Therefore, a numerical analysis is done to confirm the feasibility and performance of the proposed hybrid sample container retriever in the Mars space environment.

This OS has three permanent magnets on the bottom of one side to benefit the flux pinning effect in the docking phase, as shown in Fig. 2. If the OS is used for the MSR mission, however, the angular velocity and attitude must be controlled to safely be captured using the flux pinning effect. As a control method for the OS, the coulomb force is used to control the states of the OS, which does not need to have any actuators. The OS is electrostatically tugged into the range of the flux pinning effect while controlling the attitude and angular velocity using the coulomb force. Finally, rendezvous docking using the FPI is operated when the OS enters into the range of the flux pinning effect. In this section, the fundamental information required to use the electrostatic control system is given for the proposed sample container retriever system.

A. Debye Shielding on Martian Low Orbits

When the electrostatic interaction is considered in a plasma environment, the Debye shielding effect occurs. If the interaction between charged particles is considered in a vacuum environment, the coulomb force (related to Laplace potential field) is not interrupted by the Debye shielding effect [25–27]. Thus, the Debye length must be considered when evaluating the electrostatic interaction between infinite charged bodies [28–32]. The Debye length is an important parameter because the electrostatic field rapidly decreases beyond this length by the Debye shielding effect. The E-field $E(\boldsymbol{r})$ of charged body A, for which the potential is V_A, is expressed in a plasma environment using the electron Debye length λ_D as follows:

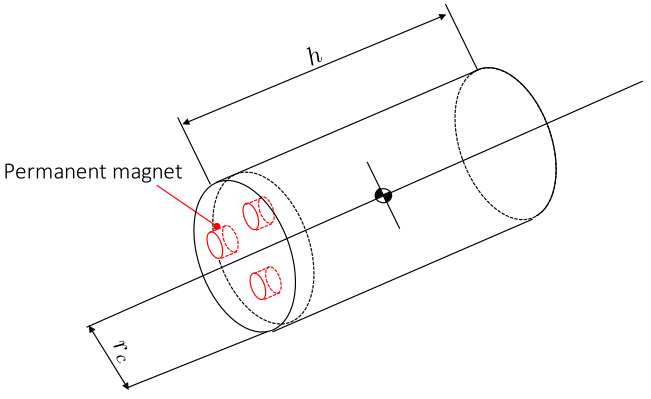

Fig. 2 Cylindrical sample container configuration.

$$E(\boldsymbol{r}) = -\nabla_r \boldsymbol{\phi}(\boldsymbol{r}) = \frac{V_A R_A}{r^2} e^{-(r-\boldsymbol{R}_A)/\lambda_D}\left(1 + \frac{\boldsymbol{r}}{\lambda_D}\right) \tag{1}$$

where $\boldsymbol{r}$ and $\boldsymbol{R}_A$ are the distances from the center of charged body A and the radius of the body, respectively. This expression shows that the E-field decreases exponentially as the distance $\boldsymbol{r}$ exceeds the electron Debye length. The electron Debye length can be expressed as

$$\lambda_D = \sqrt{\frac{\epsilon_0 T_e}{n_e q_e^2}} \tag{2}$$

where ϵ_0 is the permittivity of the vacuum, and q_e (in coulombs) is the electron charge. This electron Debye length depends on the density n_e [1/cm^3] and temperature T_e (in electron volts) of an electron. The Debye length can be long on high-altitude orbits because electrons exist with low density and high temperature [33,34]. Therefore, it has been considered that detumbling methods and formation flying technologies using the coulomb force are used on Geosynchronous Orbit (GEO) [19,20,28,35,36] for Earth applications.

The electron Debye length considers only electron physics although electrons and ions are mixing neutrally in a plasma. This means the expression considers only the case of the plasma physics in timescales, which is longer than the motion of the ions [37]. For this assumption, the electron Debye length is not useful to estimate the range of the coulomb force for this system. Moreover, this electron Debye length cannot take into account the interaction between finite bodies. Therefore, the Debye–Hückel model is applied to estimate the Debye length by taking account of the size of charged bodies. This models the impact of the Debye length more accurately. The effective Debye length λ_D is proposed to solve the range of the coulomb force for finite charged bodies [38]. It is assumed that the electron Debye length λ_D is related lineally to the effective Debye length $\bar{\lambda}_D$ using a scaling factor σ as

$$\bar{\lambda}_D = \sigma \lambda_D \tag{3}$$

Assuming the cylindrical OS is launched to orbits about 600 km in altitude above Mars, the plasma characteristics are dense and low energy as compared with higher orbits such as GEO. The denser and cooler plasma characteristics of low orbits reduce the Debye length magnitude. To investigate the effective Debye length on the orbits, the orbiter is approximated as a sphere. Values of the plasma parameters at 600 km are defined by referring to data of Viking I, Mars Atmosphere and Volatile EvolutioN, and Mars Advanced Radar for Subsurface and Ionosphere Sounding missions [39–44]; and those parameters are shown in Table 1. The σ value is solved as in Fig. 3 using those parameters. As seen in Fig. 3, the green surface is the scaling factor σ on the Martian orbits at 600 km. This scaling factor intricately depends on not only parameters of the orbiter but also the characteristics of plasma and the currents generated on the orbiter. A regression analysis is conducted to calculate the effective Debye length using the result of Fig. 3 [25]. The scaling factor σ depending on the radius R_A and the potential ϕ of the orbiter is expressed as

$$\sigma(\phi, R_A) = (1 + \phi) f(\phi, R_A) + (1 + R_A) \log \phi \tag{4}$$

where $f(\phi, R_A)$ is given as a first-order polynomial function. The scaling factor σ is derived as the following expression to fit numerically computed scaling factor σ:

Table 1 Parameters of particles in plasma on Martian orbits at 600 km

Particle	Density 1/cm^3	Temperature eV
Ion	50	0.63
Electron	20	0.42
Photon	— —	0.4

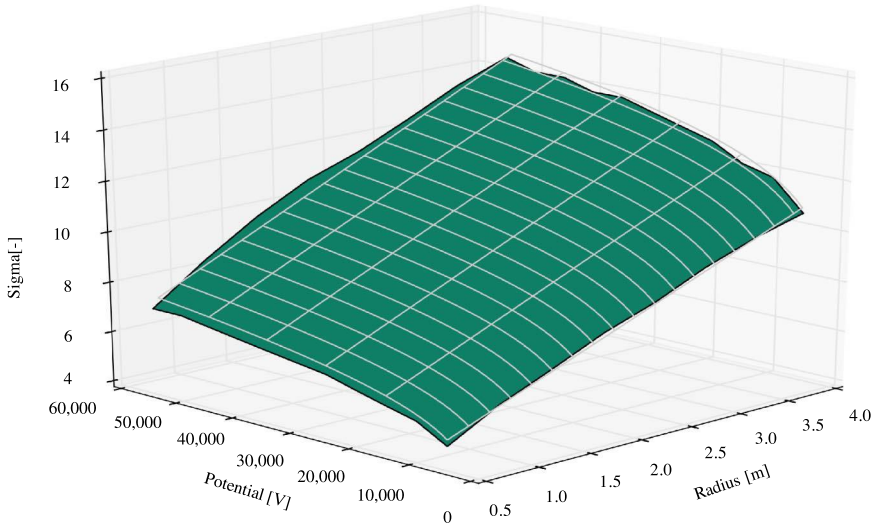

Fig. 3 Scaling factor σ depending on the potential and radius of the spherical orbiter.

$$\sigma = -2.6221 + 1.758 \times 10^{-5}\phi - 5.28 \times 10^{-11}\phi^2 - 1.73 \times 10^{-7}R\phi + 0.4296R + 0.7826 \log \phi + 0.1434R \log \phi \tag{5}$$

This Eq. (5) is given by a multilinear regression model. When the effective Debye length is estimated for this proposed system on the target orbits, this σ using Eq. (5) has a tremendous advantage because the scaling factor σ allows us to rapidly calculate the effective Debye length. This regression expression is shown in Fig. 3 as a white line and is evaluated as the coefficient of determination $R^2 = 0.991$. The dependence on the size and potential of the spherical orbiter is expressed as in Fig. 4 using the regression expression. The bigger the radius and the higher the potential of the orbiter, the larger the effective Debye length. Although the size of the orbiter is limited by the payload fairing of a rocket, the effective Debye length becomes over 10 m if the size of an orbiter is allowed by the rocket's fairing according to Fig. 4. However, the effective Debye length is still a short distance as compared with the GEO's Debye length, which is over 100 m.

B. Power Requirement to Operate the Proposed System

Ions and electrons must be emitted with enough energy to leave from the E-field of the Martian sample return orbiter. Otherwise, those particles can come back to the MSR orbiter. The orbiter in this study has two ion guns and an electron gun to change the potential of the cylindrical OS and itself. One of ion guns is directed to the OS to control the potential. The other ion gun and electron gun are used to control the potential of the orbiter. The orbiter is charged up by several factors in the plasma environment [33,34]. The currents caused by several factors flow on the OS and the orbiter as well, and the factors are divided into two different process, to charge of a body in plasma, which are called the primary charging process and the secondary emission in this paper. The primary charging process is caused by not only the plasma environment but also by photoelectrons from the solar activity. Plasma electrons, ions, and photoelectrons hit a space object and result in generating currents on a body. In addition to the primary charging process, secondary emission occurs when the primary ion, which is shot from an ion gun on the orbiter, is impacted into the potential barrier of the OS; and then secondary electrons are emitted. This emission of secondary electrons also generates currents on the body. It is assumed that the potential of the OS is maintained to be constant. Only the potential of the orbiter is controlled in this paper. Those currents generated by the impact of those particles are expressed numerically. Those expressions are shown, and the required power to operate the proposed retrieval system is estimated in this section.

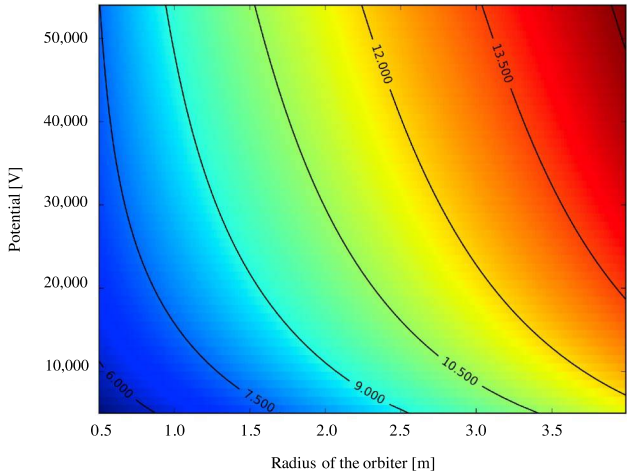

Fig. 4 Effective Debye length depending on the potential and radius of the spherical orbiter.

A photoelectron current is generated on body A, which receives the energy of the solar light. This photoelectron current is expressed as

$$\begin{aligned} I_{\mathrm{ph}}(\phi_A) &= j_{\mathrm{ph},0}A_{\perp}e^{-\phi_A/T_{\mathrm{ph}}} \quad \phi_A > 0 \\ &= j_{\mathrm{ph},0}A_{\perp} \quad \phi_A \le 0 \end{aligned} \tag{6}$$

where ϕ_A is potential of body A; T_{ph} is the temperature of the photoelectrons; and $A_{\perp} = \pi r_o^2$, which r_o is a radius of spherical body A, is a cross-sectional area exposed to solar radiation. Note that $j_{\mathrm{ph},0}$ is the photoelectron current and depends on the distance from the sun as [45]

$$j_{\mathrm{ph},0} = j'_{\mathrm{ph},0}\left(\frac{r_e}{r_m}\right)^2 \tag{7}$$

where $r_m = 1.5$ Astronomical Unit (AU) is the distance between Mars and the sun, $r_e = 1.0$ AU is the distance between the Earth and the sun, and $j'_{\mathrm{ph},0}$ is the photoelectron current on an orbit around the Earth. As the photoelectron current on orbits around the Earth is assumed to be 20 $\mu\mathrm{A/m^2}$, 8.9 $\mu\mathrm{A/m^2}$ is derived as the current on Martian orbits [34,46]. From this result, the photoelectron current is defined as 10 $\mu\mathrm{A/m^2}$ by taking into account a bias in this paper.

The electron current is modeled as [47]

$$I_e(\phi_A) = -\frac{Aqn_e\omega_e}{4}e^{\phi_A/T_e} \quad \phi_A < 0$$
$$= -\frac{Aq_en_e\omega_e}{4}\left(1+\frac{\phi_A}{T_e}\right) \quad \phi_A \geq 0 \tag{8}$$

where $A = 4\pi r_o^3$ is the surface area of body A, q is the elementary charge, n_e is the density of electrons, and $\omega_e = \sqrt{8T_e/\pi m_e}$ is the thermal velocity of electrons. The mass of the electron is $m_e = 9.11 \times 10^{-31}$ kg.

Similar to the electron current, the ion current is modeled as [47]

$$I_i(\phi_A) = \frac{Aqn_i\omega_i}{4}e^{\phi_A/T_i} \quad \phi_A > 0$$
$$= \frac{Aq_in_i\omega_i}{4}\left(1-\frac{\phi_A}{T_i}\right) \quad \phi_A \leq 0 \tag{9}$$

where n_i is the density of ions, and $\omega_i = \sqrt{8T_i/\pi m_i}$ is the thermal velocity of ions. T_i and m_i are the temperature and mass of the ions respectively. The mass of ions is 1.67×10^{-27} kg.

Electrons must be emitted from the orbiter with enough energy to intrude in the potential barrier of the OS. When the OS receives electrons emitted by the electron gun on the orbiter, the electron current $I_{\mathrm{tr},2}$ flows. This electron current on the OS depends on the energy of the electron gun E_{tr} and both the potential of the orbiter ϕ_o and the OS ϕ_s. The current $I_{\mathrm{tr}2}$ is modeled as follows:

$$I_{\mathrm{tr}2}(\phi_s) = -\delta I_{\mathrm{tr}} \quad q(\phi_s - \phi_o) < E_{\mathrm{tr}}$$
$$= 0 \quad q(\phi_s - \phi_o) \geq E_{\mathrm{tr}} \tag{10}$$

where I_{tr} is the beam current operated by the orbiter. The parameter δ is the efficiency of the transfer, and this coefficient is dealt with as 1.0 in this paper. It is assumed that the parameter of the ion gun's energy depends on the potential of the orbiter, and it is expressed as in Eq. (10).

The secondary effect current flows on the OS when it receives ions from the orbiter. This current can be calculated using the following expression as [48]

$$I_{\mathrm{SEE}}(\phi_s) = -4Y_M I_{\mathrm{tr}2}(\phi_s)K \quad \phi_A < 0 \text{ and } I_{\mathrm{tr}} > 0$$
$$= 0 \quad \phi_A \geq 0 \text{ or } I_{\mathrm{tr}} < 0 \tag{11}$$

where

$$K = \frac{E_{\mathrm{eff}}/E_{\max}}{(1 + E_{\mathrm{eff}}/E_{\max})^2} \tag{12}$$

and

$$E_{\mathrm{eff}} = E_{\mathrm{tr}} - q(\phi_s - \phi_o) \tag{13}$$

Y_M is the maximum yield of secondary electron production; and $E_{\max}$ is the maximum impact energy, for which the values depend on the material consisting of the OS. In this study, aluminum is used for the material of the OS, and then $Y_M = 2$ and $E_{\max} = 300$ eV.

In this study, the potential of the OS is maintained by achieving the net current balance on the OS. The ion gun on the orbiter operates to make the potential of the OS constantly positive. Then, the ion guns must operate to meet the following condition:

$$I_{e,s} + I_{\mathrm{tr}2,s} = 0 \tag{14}$$

where $I_{e,s}$ and $I_{\mathrm{tr}2,s}$ are the electron current and the beam current on the OS. If the potential of the orbiter is positive, the ion current I_i, the photoelectron current I_{ph}, and the secondary effect $I_{\mathrm{SEE},s}$ can be neglected. If the orbiter's potential becomes negative, the current balance expression is expressed as

$$I_{e,s} + I_{i,s} + I_{\mathrm{SEE},s} + I_{\mathrm{ph},s} + I_{\mathrm{tr}2,s} = 0 \tag{15}$$

In addition, the ion and electron guns to control the potential of the orbiter also must operate under the following condition:

$$I_{\mathrm{ex}} = -I_{\mathrm{tr}} - I_{\mathrm{ph},o} - I_{e,o} - I_{i,o} \tag{16}$$

The ion or electron guns must emit the current I_{ex} to control the potential. The power to transfer ions is a function of the beam energy and the transfer current of the ion gun on the orbiter:

$$P_{\mathrm{tr}} = \frac{E_{\mathrm{tr}}|I_{\mathrm{tr}}|}{q_b} \tag{17}$$

If a radius of the orbiter gets bigger, then higher currents are generated by the collision of those particles. This means the higher total operational power for the ion and electron guns is required to control the potential of the orbiter and the OS as well in the plasma environment. In this paper, the radius of the orbiter is defined as 1.0 m; the maximum potential that the orbiter can use is ± 10 kV, and the relative distance between the orbiter and the OS is fixed as 3.0 m, which is in the range of the effective Debye length. The shape of the OS is a cylinder shape, as in Fig. 2; and the height h and radius r_c are defined as 0.3 and 0.05 m, respectively.

When an operation of the proposed system is conducted with $\phi_s = +10$ kV and $\phi_o = -10$ kV, the orbiter must transfer and emit ions to achieve the potential of the OS and the orbiter itself. If a positive potential of the orbiter of $\phi_o = +10$ kV is required while the potential of the OS is maintained as positive at $\phi_s = +10$ kV, the orbiter must emit electrons. As seen in Table 2, 77.1 W is required for the operation of $\phi_s = +10$ kV and $\phi_o = -10$ kV; and the operation of $\phi_s = +10$ kV and $\phi_o = +10$ kV requires 1029 W. The maximum total power is estimated roughly as 1029 W under the condition of the size and the maximum potential. However, it is expected that the maximum required power can decrease when both of OS and the orbiter are positively charged up. The different polarities of those charged bodies are desirable because the attitude of the OS must be aligned to the orbiter to dock using the flux pinning interface. As seen in Fig. 5, the equilibrium attitude can be controlled by the potential of the orbiter if the potential of the OS is constantly positive. If a repulsive force is operated between the OS and the orbiter, then the OS behaves to achieve the vertical equilibrium attitude because the OS is always pushed (as in Fig. 5a). However, a different sign of the potential makes the bottom of the OS point toward the orbiter (as in Fig. 5b). From the behavior, it is expected that the maximum positive power of 1029 W is not required if the potential of the OS is maintained as +10 kV because the different potential is desirable to align the attitude of the OS. Therefore, the maximum power will be rewritten in the Sec. V about the control results.

III. Force Distribution Between the MSR Orbiter and the Cylindrical Martian OS

Both the coulomb force and the flux pinning force are used to fetch a cylindrical Martian OS using the proposed method. The pinning

Table 2 Required total power to operate the hybrid sample container retriever

Particle	Transfer	External	Total power
— —	$I_{\mathrm{tr}} = 0.91$ mA	$I_{\mathrm{ex}} = -5.89$ mA	77.1 W
$\phi_s = +10$ kV	$E_{\mathrm{tr}} = 20$ keV	$E_{\mathrm{ex}} = 10$ keV	— —
$\phi_o = -10$ kV	$P_{\mathrm{tr}} = 18.2$ W	$P_{\mathrm{ex}} = 58.9$ W	— —
— —	(i^+)	(i^+)	— —
— —	$I_{\mathrm{tr}} = 0.91$ mA	$I_{\mathrm{ex}} = 102.9$ mA	1029 W
$\phi_s = +10$ kV	$E_{\mathrm{tr}} = 0$ keV	$E_{\mathrm{ex}} = 10$ keV	— —
$\phi_o = +10$ kV	$P_{\mathrm{tr}} = 0$ W	$P_{\mathrm{ex}} = 1029$ W	— —
— —	(i^+)	(e^-)	— —

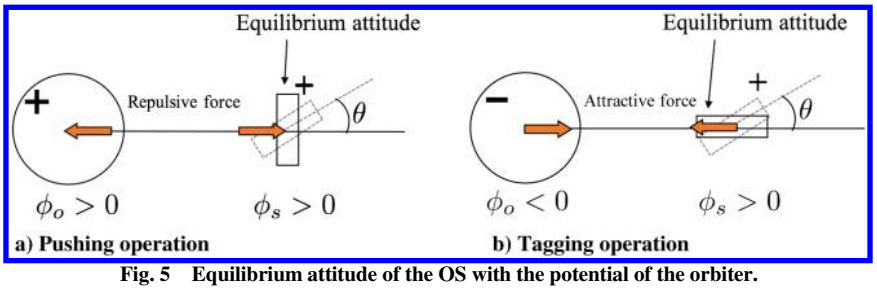

Fig. 5 Equilibrium attitude of the OS with the potential of the orbiter.

force acts in close distance, although the force is depending on the parameters of a type-II superconductor (SC) and a permanent magnet (PM), which are used for this proposed system. This force behaves repulsively before the external magnetic flux intrudes into a SC that is cooled below the critical temperature because of the Meissner effect. Once the external magnetic flux is pinned in the cooled SC, the force works as a retentive force called the flux pinning force. This effect allows us to maintain relative states between a material generating magnetic flux, which is a PM in this paper, and a cooled SC with six degrees of freedom passively. The coulomb force is used to control relative states between the cylindrical OS and the orbiter before catching the OS using the flux pinning force. The Lorentz force introduces a disturbance, however, because the OS has three PMs and is approaching the orbiter with a velocity. Therefore, the Lorentz force and the flux pinning force are considered to be acting on the cylindrical Martian OS and the Martian sample return orbiter in the effective Debye length. This section shows the force distribution depending on the relative distance between the OS and the MSR orbiter.

A. Pinning Force

The frozen image model is used to estimate the pinning force in this paper [49,50]. The pinning force works retentively as the external magnetic flux is pinned in a cooled type-II superconductor. This model can calculate the pinning force easily under assumptions that a type-II superconductor is bigger than a material generating magnetic flux, and it is an ideal material. Two images, which are called the frozen image and the mobile image, are used to calculate the pinning force, as shown in Fig. 6. Those images are generated when a SC is cooled below a critical temperature, which depends on the type of SC. In the case of Yttrium Barium Copper Oxide (YBaCuO), the temperature is around 93 K.

The pinning force is calculated as the total magnetic force between a pinned PM and two mirror images, which are the frozen image and the mobile image, by this frozen image model. $\boldsymbol{M}_p$, $\boldsymbol{M}_f$, and $\boldsymbol{M}_m$ are magnetic moment vectors of the PM and the frozen and mobile images, respectively. The relation of those magnetic moment vectors is defined as $\boldsymbol{M}_p = \boldsymbol{M}_f = -\boldsymbol{M}_m$ if the PM moves along only the y axis and the direction of $\boldsymbol{M}_p$ is along with the y axis in Fig. 6. The magnetic moment vector is expressed as $M_p = R_p^2 \pi h_p m_z$, which includes the radius R_p, height h_p, and magnetization m_z of the PM. The magnetic force F_f between the mirror image, which are the frozen image or the mobile image, and the pinned PM is expressed as [14]

$$\boldsymbol{F}_{f,m} = \mu_0 \nabla (\boldsymbol{H}_{f,m} \cdot \boldsymbol{M}_p) \tag{18}$$

where the magnetic field generated by the frozen image $\boldsymbol{H}_{f,m}$ is

$$\boldsymbol{H}_{f,m} = \frac{1}{4\pi r_{f,m}^3} \left\{ -\boldsymbol{M}_{f,m} + \frac{(3\boldsymbol{M}_{f,m} \cdot \boldsymbol{r}_{f,m})}{r_{f,m}^2} \boldsymbol{r}_{f,m} \right\} \tag{19}$$

where $\boldsymbol{r}_{f,m}$ is the position vector from the mirror image, which is the frozen image or the mobile image, to the pinned PM. The position vectors $\boldsymbol{r}_f$ and $\boldsymbol{r}_m$ between the PM and the mirror images are expressed as

$$\boldsymbol{r}_f = \boldsymbol{r} - \boldsymbol{r}_{\mathrm{FC}} + (2\boldsymbol{a} \cdot \boldsymbol{r}_{\mathrm{FC}})\boldsymbol{a} \tag{20}$$

$$\boldsymbol{r}_m = 2(\boldsymbol{a} \cdot \boldsymbol{r})\boldsymbol{a} \tag{21}$$

where $\boldsymbol{r}$ is the position vector between the PM and a point located on the surface of the cooled SC, $\boldsymbol{r}_{\mathrm{FC}}$ is the position vector between the PM

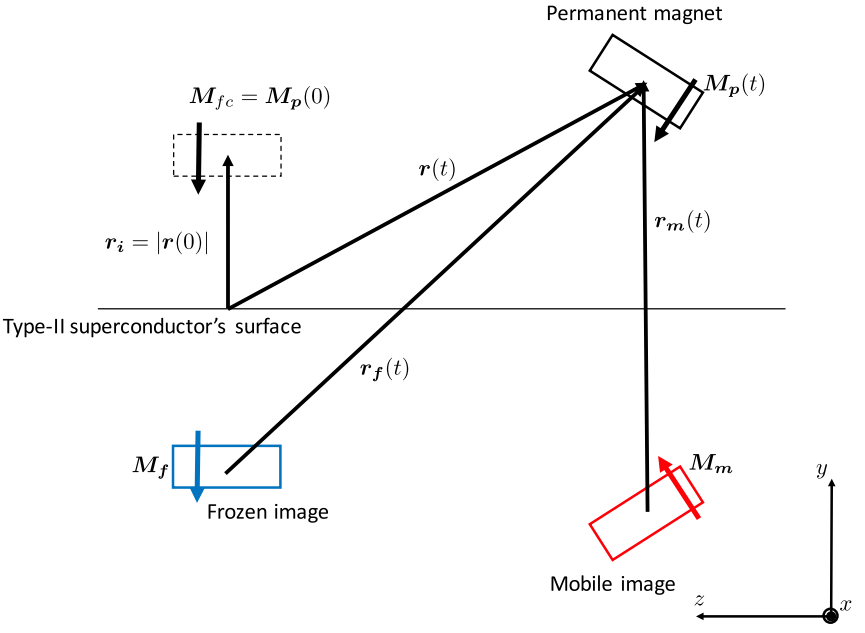

Fig. 6 Frozen image model.

at an initial position and the point, and $\boldsymbol{a}=[0,1,0]^t$ is a unit vertical vector on the surface of the SC. Finally, the pinning force $\boldsymbol{F}_p$ is expressed as the total magnetic force between the PM and the mirror images:

$$\boldsymbol{F_p} = \boldsymbol{F_f} + \boldsymbol{F_m} \tag{22}$$

If three permanent magnets are put on the bottom of the OS as vertices of the equilateral triangle (as in Fig. 2), then the vertical pinning force is written readily as [51]

$$F_{pz} = \frac{9\mu_0 M_z^2}{2\pi}\left[\frac{1}{\{(2z_i+z)\}^4} - \frac{1}{(2z_i+z)^4}\right] \tag{23}$$

B. Lorentz Force

The Lorentz force $\boldsymbol{F}_{L,s}$ works on a charged body due to the external electrostatic field $\boldsymbol{E}_s$ and the magnetic field $\boldsymbol{B}_m$. The force behaves on the cylindrical OS with three PMs as

$$\boldsymbol{F}_{L,s} = -q_o\{\boldsymbol{E}_s + \boldsymbol{v}\times\boldsymbol{B}_m\} \tag{24}$$

where q_o and $\boldsymbol{v}$ denote the charge of the MSR orbiter and a relative velocity between the orbiter and the OS. In this paper, the first term of $-q_o\boldsymbol{E}_s$ in Eq. (24) is called the coulomb force (electrostatic force) and second term of $-q_o(\boldsymbol{v}\times\boldsymbol{B}_m)$ is called the magnetic force. The multisphere model (MSM) is used for calculating the coulomb in Eq. (24) affecting between the OS and the orbiter [18]. The coulomb force can be calculated using the finite element model (FEM); however, the FEM requires a high calculation cost even though the FEM has high fidelity [22]. The MSM defines a charged body as a mass of spheres and calculates the electrostatic interaction between the charged bodies constructed by those spheres. In this calculation, the orbiter and the OS are assumed as one sphere and three spheres, as shown in Fig. 7. The spheres constructing the OS are dubbed as spheres 1, 2, and 3, respectively. The potential of the spheres q_i interacts with others, and the interaction can be defined as follows:

$$\phi_i = k_c\frac{q_i}{R_i} + \sum_{j=1,j\neq i}^{m} k_c\frac{q_j}{r_{i,j}} \tag{25}$$

where ϕ_i is the potential of sphere i, k_c is the coulomb's constant, R_i is the radius of sphere i, and $\boldsymbol{r}_{i,j}$ is the distance between the centers of spheres i and j. The vector $\boldsymbol{r}_{i,j}$ is defined as $\boldsymbol{r}_{i,j} = \boldsymbol{r}_j - \boldsymbol{r}_i$, where $\boldsymbol{r}_i$ and $\boldsymbol{r}_j$ are the position vectors from the center of the total body (which consists of those spheres) to spheres i and j, respectively. Equation (25) can be rewritten using the position-dependent capacitance (PDC) matrix C_M as

$$\boldsymbol{\phi} = k_c[C_M]^{-1}\boldsymbol{q} \tag{26}$$

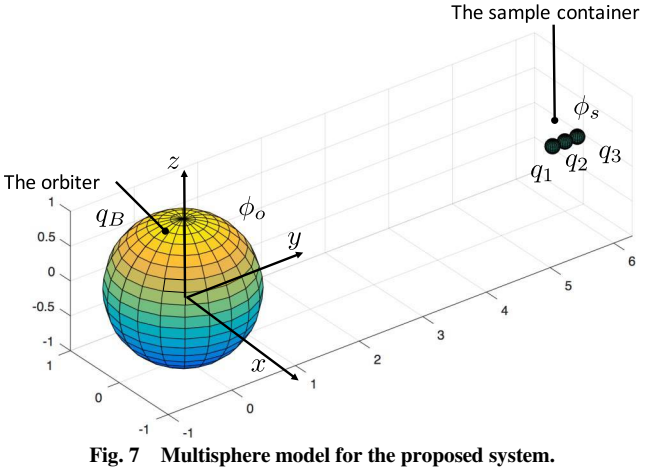

Fig. 7 Multisphere model for the proposed system.

where $\boldsymbol{\phi}=[\phi_s,\phi_s,\ldots\phi_o]^t$ and $\boldsymbol{q}=[q_1,q_2,q_3,\ldots q_B]^t$ are collections of potentials and charges in this system. The PDC matrix can be arranged as follows:

$$[C_M]^{-1} = \begin{bmatrix} 1/R_1 & 1/r_{1,2} & \ldots & 1/r_{1,n} & 1/r_{1,B} \\ 1/r_{2,1} & 1/R_2 & \ddots & \vdots & \vdots \\ \vdots & \ddots & \ddots & \vdots & \vdots \\ 1/r_{n,1} & \ldots & \ldots & 1/R_n & 1/r_{n,B} \\ 1/r_{B,1} & \ldots & \ldots & 1/r_{B,n} & 1/R_B \end{bmatrix} \tag{27}$$

The charge of each sphere depending on the potential is given using Eq. (26). Finally, the coulomb force working on the OS is expressed as

$$\boldsymbol{F}_{c,s} = -k_c q_o \sum_{i1=}^{n}\frac{q_i}{r_{i,B}^3}\boldsymbol{r}_{i,B} \tag{28}$$

C. Forces Distribution

The relative velocity between the Martian OS and the MSR orbiter is assumed to be $v=[0,10,0]^t$ m/s to calculate the Lorentz force. The radius, height, and magnetization of the PMs on the cylindrical OS are 0.01 m, 0.01 m, and 7.41×10^5 A/m, respectively; and three magnets are mounted on the OS. It is assumed that the flux pinning effect occurs between a type-II superconductor on the MSR orbiter and the PMs on the OS at 0.1 m.

The results of the force distribution map between the OS and the obiter are shown in Fig. 8. As seen in Fig. 8a, the coulomb force is dominant in region A and the pinning force gets bigger than the other forces in region B after being pinned. Therefore, only the coulomb force essentially affects the OS in region A, where the relative distance is a few meters. In region C, the pinning force is increasing exponentially as the relative distance gets closer, as seen in Fig. 8b. From those results, the coulomb force cannot control the relative distance between the OS and the MSR orbiter after the PMs are pinned in the SC in regions B and C. When it is required that the position of the OS is changed after being pinned, the electromagnetic coils (which are mounted on the orbiter for the FPI docking system) must be operated. In all of the region, the magnetic force can not be neglected if the magnetic moment of the PMs and the relative velocity are large enough.

It is noted that a smaller pinning force than the calculated result operates between the MSR orbiter and the OS because of the difference in cooling processes for type-II superconductors. There are two ways to generate the flux pinning effect, which are called field cooling (FC) and zero field cooling (ZFC). FC is the way that a SC is cooled below a critical temperature while applying the external magnetic flux to the SC before cooling. The other way is ZFC that the external magnetic flux is forcibly intruded into a SC after cooled it below critical temperature. This frozen image model can calculate the FC pinning force rather than the ZFC pinning force. Therefore, if ZFC is used as the cooling method for type-II superconductors to perform docking with the OS, the calculated pinning force gets smaller than the calculated result in this section.

The coulomb force dominantly works in the distance over 0.9 m in region A, as shown in Fig. 8. To design a controller to stabilize the states of the OS, it is considered that the relative distance between the OS and the orbiter is fixed at 3.0 m, which means that the magnetic force and the pinning force are sufficiently smaller than the coulomb force.

IV. Nonlinear Controller Design

A. Equation of Rotational Motion for the Proposed Sample Container Retriever

It can be assumed that only the coulomb force affects the OS and the MSR orbiter if the relative distance can be kept in region A of

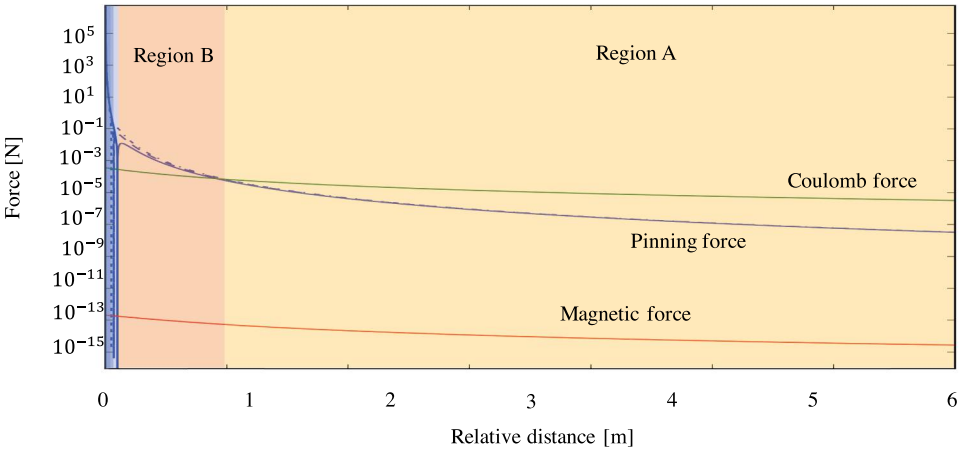

a) Force distribution in the relative distance of 6.0 m

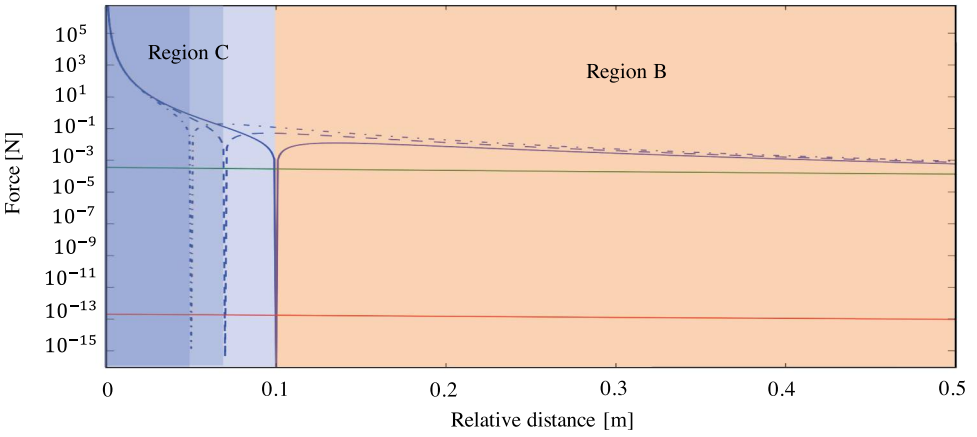

b) Force distribution in the relative distance of 0.5 m

Fig. 8 Force distribution from the surface of the MSR orbiter.

Fig. 8. The orbiter uses thrusters to maintain the relative distance. The coulomb force is used to control the attitude and angular velocity of the OS. The torque working on the OS $\boldsymbol{L}_{\text{cx}}$ can be expressed as

$$\boldsymbol{L}_{\text{cx}} = -k_c q_B \sum_{i=1}^{n} \frac{q_i}{r_{i,B}^3} \boldsymbol{r}_i \times \boldsymbol{r}_{i,\boldsymbol{B}} \tag{29}$$

where $\boldsymbol{r}_{i,\boldsymbol{B}}$ is $\boldsymbol{r}_{\boldsymbol{B}} - \boldsymbol{r}_i$, and $\boldsymbol{r}_{\boldsymbol{B}}$ is the position vector from a sphere of the OS to the orbiter. It is considered that the OS rotates around the x axis for simplicity in this paper as seen in Fig. 9. The torque with respect to the x axis is calculated as in Fig. 10 using the expression. The torque is modeled by referring to the result of the coulomb torque as

$$L_x = \gamma f(\phi) g(\theta_x) \tag{30}$$

where $f(\phi) = \phi$ is a function depending on the potential of the orbiter. Also, $g(\theta_x) = \sin 2\theta_x$ expresses the dependence of the torque on angle θ_x. Note that γ is a scaling factor and depends on the signs of the potential as

$$\gamma(\text{sign}(\phi)) \begin{cases} \gamma_n & \phi < 0 \\ \gamma_p & \phi > 0 \end{cases} \tag{31}$$

This scaling factor γ is always positive, but the value is changed by the sign of the potential. If the rotation motion around only the x axis is considered, the motion of the equation is given as

$$J_{xx}\ddot{\theta}_x = L_x \tag{32}$$

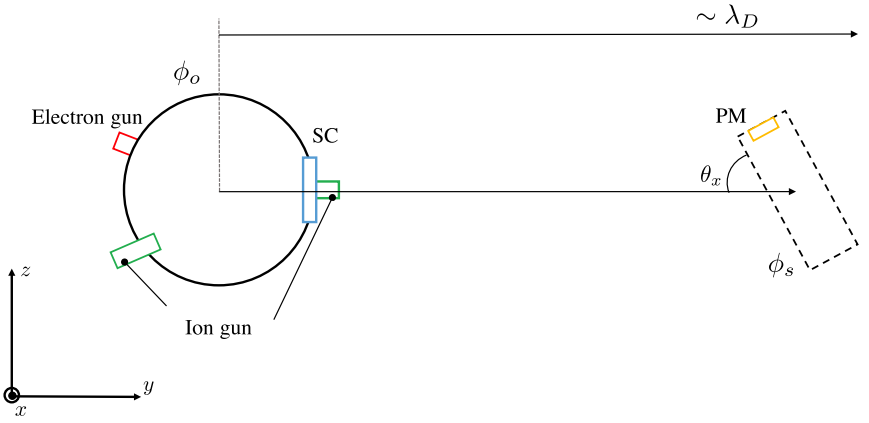

Fig. 9 Proposed retrieval system model to fetch the Martian orbital sample container.

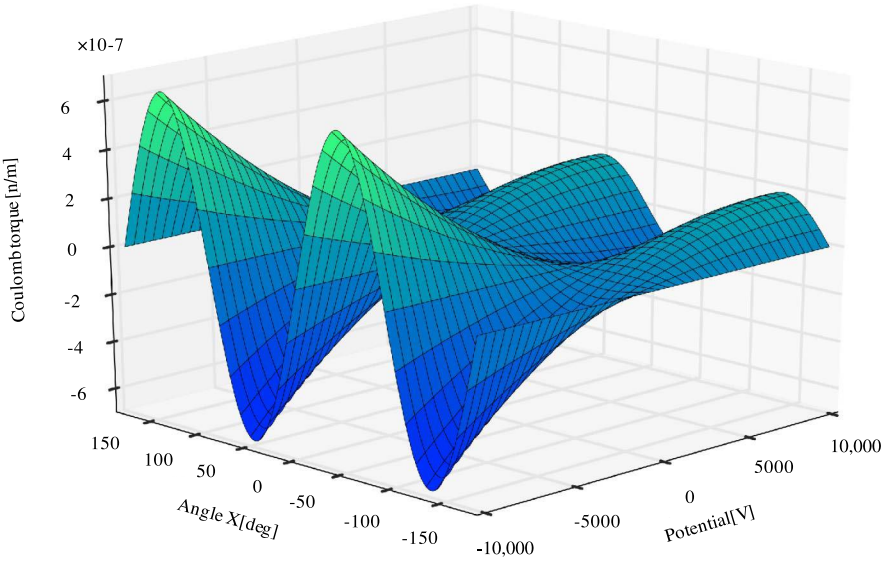

Fig. 10 Coulomb torque calculated by multisphere model when the relative distance between the OS and the orbiter is 3.0 m.

where J_{xx} is the inertia of the orbiter. When the electrostatic interaction acts between the OS and the orbiter, the Euler equation can be written as the following expression by substituting the modeled coulomb torque:

$$J_{xx}\ddot{\theta}_x - \gamma f(\phi) g(\theta_x) = 0 \tag{33}$$

A nonlinear controller is designed to converge the angular velocity and the attitude of the OS around the x axis in the following section.

B. Stability Analysis for the Controller

In this section, a nonlinear controller is designed. The controller must make the states of the OS converge to the desired alignment, which means $\theta_x \to 0$ and $\dot{\theta}_x \to 0$. A Lyapunov function is used to understand the stability of the nonlinear controller. A Lyapunov function candidate is designed as

$$V(\boldsymbol{\theta}) = \ell_n(1 + \sin^2\theta_x)\frac{\gamma\phi_{\max}}{\beta} + \frac{1}{2}J_{xx}\dot{\theta}_x^2 \tag{34}$$

where $\boldsymbol{\theta} = (\theta_x, \dot{\theta}_x)$, β is a scaling factor, and $\phi_{\max}$ is the maximum potential of the orbiter. This Lyapunov function $V(\boldsymbol{\theta})$ is zero when $\boldsymbol{\theta} = 0$, and $V(\boldsymbol{\theta}) \geq 0$ in the range of ± 90 deg, as seen in Fig. 11. When the attitude of the OS is beyond this range of ± 90 deg, the following sequence must be conducted to make the Lyapunov function candidate positive semidefinite:

$$\begin{aligned} \theta_x(t + dt) &= \theta_x(t) - 180 \quad \theta_x > 90 \\ \theta_x(t + dt) &= \theta_x(t) + 180 \quad \theta_x < -90 \end{aligned} \tag{35}$$

The first derivative Lyapunov function is given as

$$\dot{V}(\boldsymbol{\theta}) = \gamma\left[\frac{\phi_{\max}}{\beta(1 + \sin^2(\theta_x))} + f(\phi)\right]\dot{\theta}_x \sin(2\theta_x) \tag{36}$$

The Mukherjee and Chen (M&C) theorem is employed to design the controller that allows the attitude and angular velocity to be asymptotically stable. The first derivative Lyapunov function $\dot{V}(\boldsymbol{\theta})$ always should be negative definite or semidefinite to make the system asymptotic stable according to the M&C theorem. Then, the controller for this retrieval system is designed as follows to make the first derivative Lyapunov function $\dot{V}(\boldsymbol{\theta}) \leq 0$:

$$\phi = -\frac{\phi_{\max}}{\beta}\left(g(\theta_x)h(\alpha\dot{\theta}_x) + \frac{1}{1 + \sin^2(\theta_x)}\right) \tag{37}$$

where α is the gain for this controller. Also, the h function is written as

$$h(\alpha\dot{\theta}_x) = \frac{\tan^{-1}(\alpha\dot{\theta}_x)}{\pi/2} \tag{38}$$

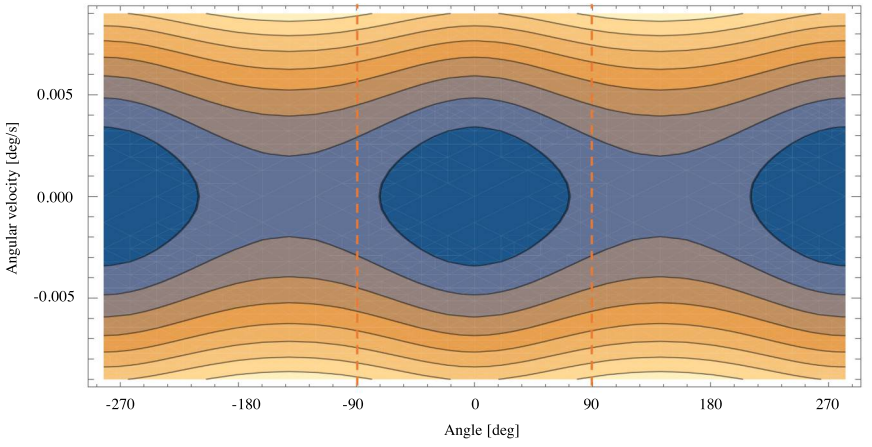

Fig. 11 Lyapunov function.

Two subsets are defined as $Z_1 = \{\boldsymbol{\theta}|\theta_x = 0\}$ and $Z_2 = \{\boldsymbol{\theta}|\dot{\theta}_x = 0\}$ to analyze the stability of the controller using the M&C theorem. When the second derivative Lyapunov function is considered in subsets $\ddot{V}(\boldsymbol{\theta}_x \in Z_1)$ and $\ddot{V}(\boldsymbol{\theta}_x \in Z_2)$, the function goes to zero. This means the Lyapunov candidate meets the asymptotic stability condition of the M&C theorem. The third derivative Lyapunov function is given as

$$\dddot{V}(\boldsymbol{\theta} \in Z_1) = -\frac{16\gamma\phi_{\max}}{\pi}\left\{\dot{\theta}_x^3 \tan^{-1}(\alpha\dot{\theta}_x)\right\} \tag{39}$$

$$\dddot{V}(\boldsymbol{\theta} \in Z_2) = -\frac{4\alpha\gamma^3\phi_{\max}}{\pi J_{xx}^2}, \qquad \left\{\frac{\sin^4(2\theta_x)}{(1+\sin^2(\theta_x))^2}\right\} \tag{40}$$

The third derivative Lyapunov function $\dddot{V}$ is locally negative definite; hence, it can be said that the closed-loop controller is asymptotically stable. This designed controller is used to align the attitude of the OS, and the performance is shown in next section.

V. Results

The initial angular velocity ω_0 and attitude θ_0 of the OS are set as 5 deg/s and 10 deg. The gain of the controller α is 10,000. The controller can converge the attitude into the range of ± 5 deg in 19,500 s, which is approximately 5.4 h (as in Fig. 12a). As seen in Fig. 12b, the angular velocity is also converged in the range of ± 0.02 deg/s in the same time. Although the attitude cannot be completely converged to zero, the pinning force can catch the OS because the pinning force works with any attitude of the OS if the magnetic flux of the PMs can be intruded into the SC on the orbiter. The error of the attitude of ± 5 deg is not a huge error for the flux pinning effect; therefore, the force works enough to catch the OS in space. In this simulation, the potential of the OS is maintained as positive using the ion gun on the orbiter. To direct the bottom of the OS to the orbiter, the negative potential of the orbiter is desirable when the potential of the OS is charged up as positive, as shown in Fig. 5. Referring to Fig. 5, this controller works to direct the bottom of the OS to the orbiter because the potential of the orbiter converges to a negative value, as seen in Fig. 12c. The potential of the orbiter does not require us to use the maximum positive potential as in Table 2. As the nonlinear controller works, the required maximum potential are -10 kV as negative and $+2.1$ kV as positive, respectively. Therefore, the required power calculated as in Table 2 can be rewritten. The required power can be calculated as 51.0 W with the potential of the orbiter of $+2.1$ kV. Although the calculated coulomb torque affecting between the orbiter and the OS is small in Fig. 12d, it is expected that the retrieval system can control the attitude of the OS sufficiently. However, the proposed system requires 5.4 h to converge the state of the OS into the range, and the relative distance must be maintained using the thruster during the time. According to the Mars 2020 mission report, the orbiter has big solar array panels (SAPs) for which the area is 15 m^2. In this paper, the orbiter is approximated as one sphere in the sense of the MSM. If the SAP can be designed using a material that can allow charging up, then the convergence time might be shorter than these results because the coulomb torque working on the OS increases.

The relation between the convergence time t_c (for which the attitude and the angular velocity converged in the range of ± 5 deg) and the required maximum power P_r is shown in Fig. 13. According to the result of the required power, the power for the positive potential of the orbiter is smaller than the negative potential because the retrieval system does not require positive potential operation so much if the potential of the OS is maintained as positive. Therefore, the required maximum power P_r is the power of when the

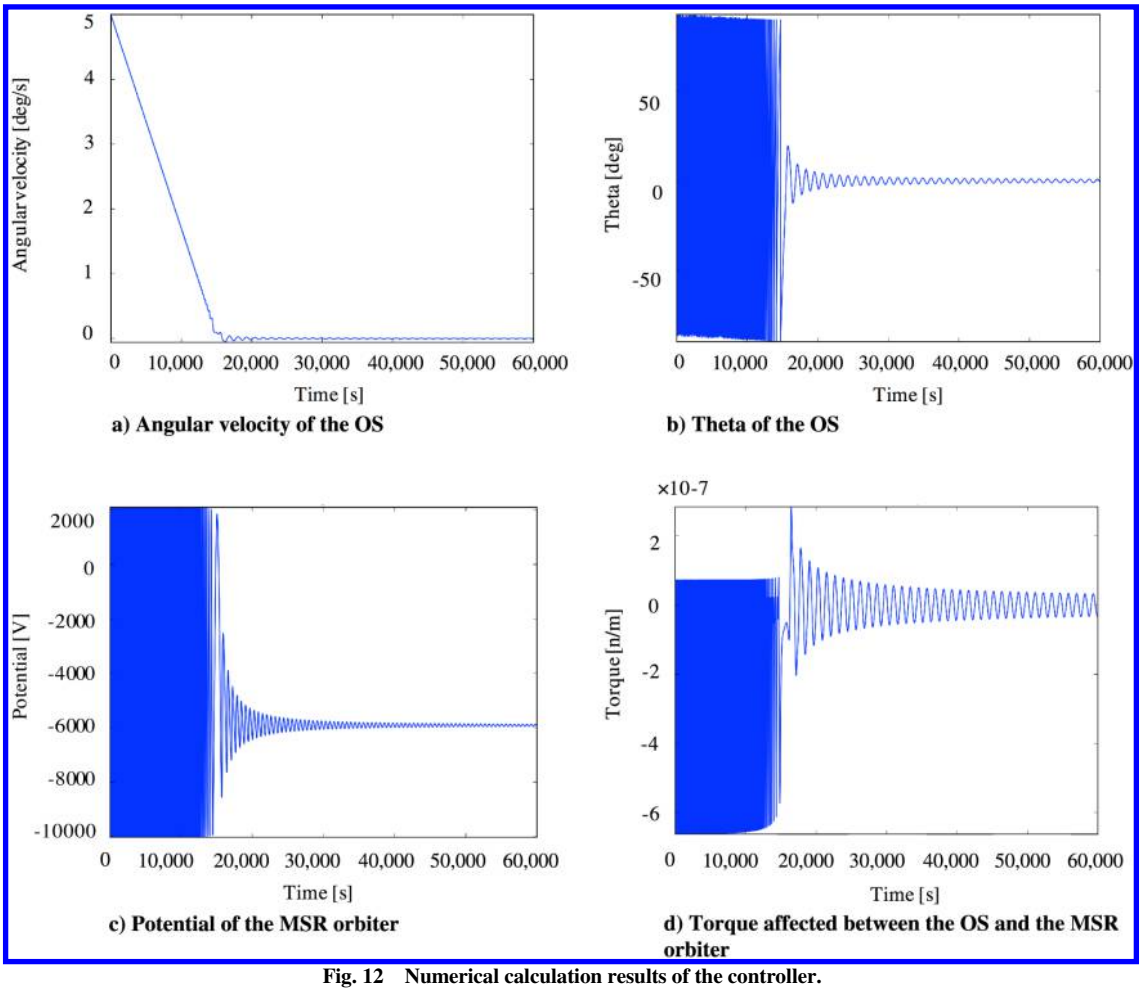

Fig. 12 Numerical calculation results of the controller.

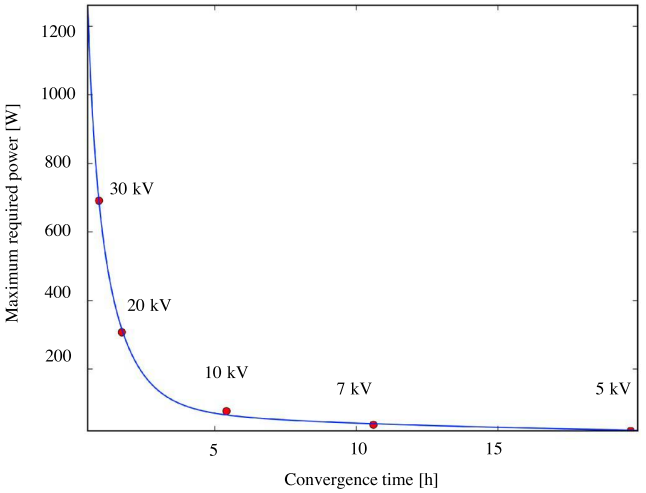

Fig. 13 Relationship between the minimum required power and the convergence time.

potential of the OS is the opposite sign of the potential of the orbiter. The relation can be expressed as follows using the regression analysis:

$$P_r = 111.10 + \frac{588.73}{\sinh(t_c)} - 30.0\log(t_c) \tag{41}$$

As seen in Fig. 13, if the orbiter can be charged up with higher potentials, the convergence time can be shorter, although higher power is required. This regression expression is useful to estimate the required power. The expression matches those points with the coefficient of determination of $R^2 = 0.999$.

VI. Conclusions

In this paper, the hybrid sample container retriever using an electromagnetic force is proposed for future sample retriever missions. To get samples from other planets, techniques for automated rendezvous and docking are important. To perform the rendezvous and docking safely on orbit, the feasibility of the rotation motion control for a cylindrical OS is discussed in this paper.

The sample container cannot be launched to a high-altitude orbit from the Martian ground because a small launcher is used; hence, there are some limitations to operating the proposed system to get the OS automatically using coulomb force in space. The first limitation is the effective Debye length. Operation of the system using the coulomb force at a low altitude should be conducted with the short effective Debye length. Therefore, it is required that an orbiter approaches the OS to get within the range of the effective Debye length. Because of the second limitation, high power is required to change the potential of the OS and the orbiter itself. The required power severely limits the maximum potential that the orbiter can use. However, the numerical results show that the proposed sample container retriever can suppress the attitude and the angular velocity of the cylindrical OS under the limitations. The convergence time takes 5.4 h to be ready for getting the OS safely and automatically. The angular velocity and attitude are converged in the ranges of ± 0.02 deg/s and ± 5.0 deg, respectively, in the time. Although the flux pinning force is affected by the error of the attitude, the flux pinning force can be used to catch the OS safely.

If the orbiter controls the potential itself in the range of ± 10 kV, the maximum required power is 1029 W with $+10$ kV operation. If the potential of the OS is maintained as positive, however, it is not required that the orbiter uses $+10$ kV operation. Therefore, the power of 1029 W is not required. In the case of the simulation presented in this paper, the power can be reduced to 51.0 W. In addition, the relation between the expected convergence time and the maximum required power was shown. The attitude and angular velocity can be rapidly converged using the designed controller if the orbiter can use higher power. However, the power that the orbiter can use for this operation is limited by the power that can be generated by the solar array panel as shown in the numerical result. From the numerical result, it can be said that the convergence time and the required power for the operation are a tradeoff relation.

Acknowledgment

An earlier version of this paper was presented at the International Workshop on Satellite Constellations and Formation Flying in 2017. The paper was not submitted officially to the workshop.

References

[1] Cazaux, C., Naderi, F., Whetsel, C., Beaty, D., Gershman, B., Kornfeld, R., Mitcheltree, B., and Sackheim, B., "The NASA/CNES Mars Sample Return–A Status Report," *Acta Astronautica*, Vol. 54, No. 8, 2004, pp. 601–617. https://doi.org/10.1016/j.actaastro.2003.07.001

[2] Clark, B. C., "Mars Sample Return: The Critical Next Step," *Acta Astronautica*, Vol. 61, Nos. 1–6, 2007, pp. 95–100. https://doi.org/10.1016/j.actaastro.2007.01.040

[3] Mattingly, R. L., "The Many Faces of the Mars Sample Return Mission Architecture," *27th Annual AAS Guidance and Control Conference*, AAS Paper 05-066, Breckenridge, 2005.

[4] Sherwood, B., "Mars Sample Return: Architecture and Mission Design," *Acta Astronautica*, Vol. 53, Nos. 4–10, 2003, pp. 353–364. https://doi.org/10.1016/S0094-5765(03)00153-X

[5] O'Neil, W. J., and Cazaux, C., "The Mars Sample Return Project," *Acta Astronautica*, Vol. 47, Nos. 2–9, 2000, pp. 453–465. https://doi.org/10.1016/S0094-5765(00)00085-0

[6] Christensen, P., and May, L., "*Mission Concept Study: Planetary Science Decadal Survey MSR Orbiter Mission*," NASA TR, March 2010.

[7] Christensen, P., and May, L., "*Mission Concept Study: Planetary Science Decadal Survey MSR Lander Mission*," NASA TR, April 2010.

[8] Dankanich, J., and Klein, E., "Mars Ascent Vehicle Development Status," *IEEE Aerospace Conference*, IEEE Publ., Piscataway, NJ, 2012. https://doi.org/10.1007/s10569-011-9387-610.1109/AERO.2012.6187295

[9] Mitcheltree, R., Braun, R., Hughes, S., and Simonsen, L., "Earth Entry Vehicle for Mars Sample Return," *51th Internatinal Astronautics Federation Congress*, International Astronautic Federation Paper IAF-00-Q.3.04, Rio de Janeiro, Brazil, 2000.

[10] Dillman, R., Laub, B., Kellas, S., and Schoenenberger, M., "Development and Test Plans for the MSR EEV," *2nd International Planetary Probe Workshop*, NASA CP-2004-213456, Moffett Field, CA, 2005.

[11] Perino, S., and Bayandor, J., "A Rapid Analysis Methodology for Earth Entry Vehicle Development," *29th Congress of the International Council of the Aeronautical Science*, International Council of the Aeronautical Sciences, St. Petersburg, Russia, 2014.

[12] Carta, R., Filippetto, D., Lavagna, M., Mailland, F., Falkner, P., and Larranaga, J., "Sample Canister Capture Mechanism for Mars Sample Return: Functional and Environmental Test of the Elegant Breaddoard Model," *Acta Astronautica*, Vol. 117, Dec. 2015, pp. 99–115. https://doi.org/10.1016/j.actaastro.2015.07.009

[13] Kornfeld, R., Parrish, J., and Sell, S., "Mars Sample Return: Testing the Last Meter of Rendezvous and Sample Capture," *Journal of Spacecraft and Rockets*, Vol. 44, No. 3, 2007, pp. 692–702. https://doi.org/10.2514/1.26098

[14] Zhu, F., Jones-Wilson, L., and Peck, M., "Capturing and Docking Spacecraft with Flux Pinned Interfaces," *67th International Astronautical Congress*, International Astronautic Federation Paper IAC-16, C1,9,4,x32785, Guadalajara, Mexico, 2016.

[15] Clerc, S., Renault, H., and Losa, D., "Control of a Magnetic Capture Device for Autonomous In-Orbit Rendezvous," *IFAC Proceedings Volumes*, Vol. 44, No. 1, Jan. 2011, pp. 2084–2089. https://doi.org/10.3182/20110828-6-IT-1002.01499

[16] Gómez, N. O., and Walker, S., "Guidance, Navigation, and Control for the Eddy Brake Method," *Journal of Guidance, Control, and Dynamics*, Vol. 40, No. 1, 2017, pp. 52–68. https://doi.org/10.2514/1.G002081

[17] Kadaba, P., and Naishadham, K., "Feasibility of Noncontacting Electromagnetic Despinning of a Satellite by Inducing Eddy Currents in Its Skin-Part I: Analytical Considerations," *IEEE Transactions on Magnetics*, Vol. 31, No. 4, 1995, pp. 2471–2477. https://doi.org/10.1109/20.390159

[18] Stevenson, D., and Schaub, H., "Multi-Sphere Method for Modeling Spacecraft Electrostatic Forces and Torques," *Advances in Space*

Research, Vol. 51, No. 1, 2013, pp. 10–20.
https://doi.org/10.1016/j.asr.2012.08.014
[19] Schaub, H., and Stevenson, D., "Prospects of Relative Attitude Control Using Coulomb Actuation," *Journal of the Astronautical Sciences*, Vol. 60, Nos. 3–4, 2013, pp. 258–277.
https://doi.org/10.1007/s40295-015-0048-y
[20] Bennett, T., and Schaub, H., "Touchless Electrostatic Three-Dimensional Detumbling of Large Axi-Symmetric Debris," *Journal of the Astronautical Sciences*, Vol. 62, No. 3, 2015, pp. 233–253.
https://doi.org/10.1007/s40295-015-0075-8
[21] Stevenson, D., and Schaub, H., "Electrostatic Spacecraft Rate and Attitude Control - Experimental Results and Performance Considerations," *Acta Astronautica*, Vol. 119, Feb. 2016, pp. 22–33.
https://doi.org/10.1016/j.actaastro.2015.10.023
[22] Stevenson, D., and Schaub, H., "Terrestrial Testbed for Remote Coulomb Spacecraft Rotation Control," *International Journal of Space Science and Engineering*, Vol. 2, No. 1, 2014, pp. 96–112.
https://doi.org/10.1504/IJSPACESE.2014.060111
[23] Bennett, T., Stevenson, D., Hogan, E., and Schaub, H., "Prospects and Challenges of Touchless Electrostatic Detumbling of Small Bodies," *Advances in Space Research*, Vol. 56, No. 3, 2015, pp. 557–568.
https://doi.org/10.1016/j.asr.2015.03.037
[24] Jones, L., Wilson, W., and Peck, M., "Design Parameters and Validation for a Non-Contacting Flux-Pinned Docking Interface," *AIAA Space 2010 Conference and Exposition*, AIAA Paper 2010-8918, 2010.
https://doi.org/10.2514/6.2010-8918
[25] Seubert, C., Stiles, L., and Schaub, H., "Effective Coulomb Force Modeling for Spacecraft in Earth Orbit Plasmas," *Advances in Space Research*, Vol. 54, No. 2, 2014, pp. 209–220.
https://doi.org/10.1016/j.asr.2014.04.005
[26] Nicholson, D., *Introduction to Plasma Theory*, Krieger, Melbourne, FL, 1992.
[27] Hogan, E., and Schaub, H., "Linear Stability and Shape Analysis of Spinning Three-Craft Coulomb Formations," *Celestial Mechanics and Dynamical Astronomy*, Vol. 112, No. 2, 2012, pp. 131–148.
https://doi.org/10.1007/s10569-011-9387-6
[28] King, L., Parker, G., Deshmukh, S., and Chong, J.-H., "Study of Interspacecraft Coulomb Forces and Implications for Formation Flying," *Journal of Propulsion and Power*, Vol. 19, No. 3, 2003, pp. 497–505.
https://doi.org/10.2514/2.6133.
[29] Wang, S., and Schaub, H., "Nonlinear Charge Control for a Collinear Fixed Shape Three-Craft Equilibrium," *Journal of Guidance, Control, and Dynamics*, Vol. 34, No. 2, 2011, pp. 359–366.
https://doi.org/10.2514/1.52117
[30] Inampudi, R., and Schaub, H., "Orbit Radial Dynamic Analysis of Two-Craft Coulomb Formation at Libration Points," *Journal of Guidance, Control, and Dynamics*, Vol. 37, No. 2, 2014, pp. 682–691.
https://doi.org/10.2514/1.55282
[31] Jones, D., and Schaub, H., "Collinear Three-Craft Coulomb Formation Stability Analysis and Control," *Journal of Guidance, Control, and Dynamics*, Vol. 37, No. 1, 2014, pp. 224–232.
https://doi.org/10.2514/1.60293
[32] Gurnett, D., and Bhattacharjee, A., *Introduction to Plasma Physics: With Space and Laboratory Applications*, Cambridge Univ. Press, Cambridge, England, U.K., 2005.
[33] Schaub, H., and Sternovsky, Z., "Active Space Debris Charging for Contactless Electrostatic Disposal Maneuvers," *Advances in Space Research*, Vol. 53, No. 1, 2014, pp. 110–118.
https://doi.org/10.1016/j.asr.2013.10.003
[34] Hogan, E., "Impact of Tug and Debris Sizes on Electrostatic Tractor Charging Performance," *Advances in Space Research*, Vol. 55, No. 2, 2015, pp. 630–638.
https://doi.org/10.1016/j.asr.2014.10.023
[35] Seubert, C., and Schaub, H., "Rotational Stiffness Study of Two-Element Tethered Coulomb Structures," *Journal of Spacecraft and Rockets*, Vol. 48, No. 3, 2011, pp. 488–497.
https://doi.org/10.2514/1.49772
[36] Seubert, C., Panosian, S., and Schaub, H., "Attitude and Power Analysis of Two-Node Multitethered Coulomb Strictire," *Journal of Spacecraft and Rockets*, Vol. 48, No. 6, 2011, pp. 1033–1045.
https://doi.org/10.2514/1.52185
[37] Hutchinson, I. H., *Principles of Plasma Diagnostics*, Cambridge Univ. Press, Cambridge, U.K., 2002.
[38] Murdoch, N., Izzo, D., Bombardelli, C., Carnelli, I., Hilgers, A., and Rodgers, D., "Electrostatic Tractor for Near Earth Object Deflection," *59th International Astronautical Congress*, International Astronautic Federation Paper IAC-08-A3.I.5, Glasgow, Scotland, U.K. 2008.
[39] Vogt, M. F., Withers, P., Fallows, K., Andersson, L., Girazian, Z., Mahaffy, P. R., Benna, M., Elrod, M. K., Connerney, J. E. P., Espley, J. R., et al., "MAVEN Observations of Dayside Peak Electron Densities in the Ionosphere of Mars," *Journal of Geophysical Research*, Vol. 122, No. 1, 2017, pp. 891–906.
https://doi.org/10.1002/2016 JA023473
[40] Benna, M., Mahaffy, P. R., Grebowsky, J. M., Fox, J. L., Yelle, R. V., and Jakosky, B. M., "First Measurements of Composition and Dynamics of the Martian Ionosphere by MAVEN's Neutral Gas and Ion Mass Spectrometer," *Geophysical Research Letters*, Vol. 42, No. 21, 2015, pp. 8958–8965.
https://doi.org/10.1002/2015GL066146
[41] Hanson, W., Sanatani, S., and Zuccaro, D. R., "The Martian Ionosphere as Observed by the Viking Retarding Potential Analyzers," *Journal of Geophysical Research*, Vol. 82, No. 28, 1977, pp. 4351–4363.
https://doi.org/10.1029/JS082i028p04351
[42] Grard, R., "Solar Photon Interaction with the Martian Surface and Related Electrical and Chemical Phenomena," *Icarus*, Vol. 114, No. 1, 1995, pp. 130–138.
https://doi.org/10.1006/icar.1995.1048
[43] Ergun, R. E., Morooka, M. W., Andersson, L. A., Fowler, C. M., Delory, G. T., Andrews, D. J., Eriksson, A. I., McEnulty, T., and Jakosky, B. M., "Dayside Electron Temperature and Density Profiles at Mars First Results from the MAVEN Langmuir Probe and Waves Instrument," *Geophysical Research Letters*, Vol. 42, No. 21, 2015, pp. 8846–8853.
https://doi.org/10.1002/2015GL065280
[44] Fowler, C. M., Andersson, L., Ergun, R. E., Morooka, M., Delory, G., Andrews, D. J., Lillis, R. J., McEnulty, T., Weber, T. D., Chamandy, T. M., et al., "The First in Situ Electron Temperature and Density Measurements of the Martian Nightside Ionosphere," *Geophysical Research Letters*, Vol. 42, No. 21, 2015, pp. 8854–8861.
https://doi.org/10.1002/2015GL065267
[45] Pfaff, R. F., Borovsky, J. E., and Young, D. T., *Measurement Techniques in Space Plasmas: Particles*, American Geophysical Union, Washington, D.C., 1998.
[46] Hogan, E., and Schaub, H., "Impacts of Hot Space Plasma and Ion Beam Emission on Electronstatic Tractor Performance," *IEEE Transactions on Plasma Science*, Vol. 43, No. 9, 2015, pp. 3115–3129.
https://doi.org/10.1109/TPS.2015.2451001
[47] Hippler, R., Pfau, S., Schmidt, M., and Schoenbach, K. H., *Low Temperature Plasma Physics: Fundamental Aspects and Applications*, Wiley, Berlin, Germany, 2001.
[48] Draine, B., and Salpeter, E., "On the Physics of Dust Grains in Hot Gas," *Astrophysical Journal*, Vol. 231, July 1979, pp. 77–94.
https://doi.org/10.1086/157165
[49] Kordyuk, A., "Magnetic Levitation for Hard Superconductors," *Journal of Applied Physics*, Vol. 83, No. 1, 1998, pp. 610–612.
https://doi.org/10.1063/1.366648
[50] Jones, L., and Peck, M., "Control Strategies Utilizing the Physics of Flux-Pinned Interfaces for Spacecraft," *AIAA Guidance, Navigation and Control Conference*, AIAA Paper 2011-6703, 2011.
https://doi.org/10.2514/6.2011-6703
[51] Shibata, T., and Sakai, S., "Design Method for the Micro Vibration Isolator Using Flux Pinning Effect for Satellites," *AIAA Astrodynamics Specialist Conference*, AIAA Paper 2016-5647, 2016.
https://doi.org/10.2514/6.2016-5647

D. Spencer
Associate Editor